Raman lidar measurements for boundary layer gradients and atmospheric refraction of millimeter-wave signals

Hallen, Hans, Philbrick, C. Russell

Hans Hallen, C. Russell Philbrick, "Raman lidar measurements for boundary layer gradients and atmospheric refraction of millimeter-wave signals," Proc. SPIE 11410, Laser Radar Technology and Applications XXV, 1141006 (19 May 2020); doi: 10.1117/12.2557158

SPIE.

Event: SPIE Defense + Commercial Sensing, 2020, Online Only, California, United States

Raman lidar measurements for boundary layer gradients and atmospheric refraction of millimeter-wave signals

Hans Hallen*[a] and C. Russell Philbrick[a,b]
[a]Department of Physics, [b]Department of Marine, Earth and Atmospheric Sciences, NC State University, Raleigh, NC 27695-8202

Abstract

The atmospheric boundary layer is typically characterized by a higher water vapor content and higher temperature than the free troposphere above it. Its height increases as the size of convection cells grow during the morning due to surface heating, stabilizes during the day, and it collapses as the energy input decreases in the evening. The marine boundary layer emphasizes these aspects. The large temperature gradients, humidity gradients and shear at the top of the boundary layer impact several processes, such as changes in both propagation properties as a function of wavelength and aerosol size distributions. We use Raman lidar to measure the gradients, and investigate several data inversion techniques to determine the best approach to obtain a high accuracy, for high SNR profiles of these gradients. Methods include anisotropic averaging between height and range, and averaging only to the level required for a specific target SNR. Examples that benefit from different time and range averaging will be given. The methods for gradient calculations and the interaction with pre- or post-averaging are also investigated. We model the impact of gradient-profile measurement from errors in the refraction of radar beams as a measure of quality requirements.

Keywords: Raman lidar, planetary boundary layer, water vapor gradients, radar propagation, data processing, 5G

1. INTRODUCTION

The propagation of electromagnetic radiation through the atmosphere is impacted by index of refraction inhomogeneities and by scattering from aerosols and droplets. When propagation is over long distances, the curvature of the Earth is also an important factor. In this paper, we consider propagation of radar and millimeter-wave (mmWave) signals. A radar system transmits a directed beam of energy. Timing of the reflection is used to determine the distance to a sensed object. Thus, both pointing and timing are important in location determination. We show below that these same parameters are the also important for mmWave communications.

The problem we are interested in is the direction in which the antenna should be pointed to reach a mobile location, and the delay time of the signal as it traverses that distance, which are both changing as a function of mobile position and motion. These are the key considerations for both types of signals, be it location (range, height) identification in radar, or the pointing angle and phase correction needed for mmWave communications. Since electromagnetic waves bend towards regions of higher index of refraction during propagation, we are interested in the gradients of quantities that impact the index of refraction. The primary drivers for the (slight) deviations in the index of refraction of air are the pressure p, temperature T, and water vapor partial pressure, including their variation in larger scale turbulent eddies present. The atmospheric pressure causes the strongest variation vertically. Lateral variations occur on very long length scales and so produce negligible gradients. Local density fluctuations due to thermal energy also occur, but are related to scattering, which simply reduces signal levels in our cases. The pressure will largely follow that of the standard reference atmosphere [1], which we assume can be corrected for automatically. In fact, we most often report the differences in the actual quantities from those of the reference atmosphere on a curved Earth. Both temperature and water vapor can vary locally, with strong gradients. These are the key parameters we will consider.

In this paper, we use real atmospheric profiles of temperature and water vapor in a ray tracing model that accounts for the curvature of the Earth. We begin with theoretical results that show interesting trends, then describe the simulations of propagation using measured vertical profiles, but assume that the same profile is found at every point of the surrounding space. We point out that strong variations are observed when using ray tracing based on atmospheric profiles taken at different positions at the same time or taken at the same position but at different times. Finally, we consider lidar measurements of the true vertical profile and its variations with position and time. These results point to break down of the simple theoretical relations seen in the laterally invariant atmospheres, and present areas for future study.

*hallen@ncsu.edu; phone 1 919-515-6314; physics.ncsu.edu/optics

Laser Radar Technology and Applications XXV, edited by Monte D. Turner, Gary W. Kamerman, Proc. of SPIE Vol. 11410, 1141006 · © 2020 SPIE
CCC code: 0277-786X/20/$21 · doi: 10.1117/12.2557158

We are also concerned with understanding the processes that become important for refraction of electromagnetic waves in the mmWave region as used for both 5G communications and radar. The frequency bands used for mmWave communications are near 26, 28, 38, and 60 GHz. The primary difference between mmWaves used in 5G and the sub-6 GHz signals that have been used prior to 5G is that the wavelength of the mmWaves is short enough that the size of an omnidirectional antenna (sub- or about-wavelength) is too small to intercept sufficient signal (maximum given by the magnitude of the Poynting vector times the antenna area) for communications. The solution is to make a larger antenna; however, this is many wavelengths in size so is inherently directional. In practice, the antennal is divided into segments and the emission/reception directions can be controlled. Thus, mmWave antennas are directional, as radar is. Timing is also crucial for mmWave communications. Most signaling schemes require accurate knowledge of the phase of the wave. Phase is tracked so that phase/magnitude constellations, as used in Pulsed Amplitude Modulation, can be separated into the sub-channels. Phase errors can be converted to timing errors by dividing by the frequency. Thus, the timing, or more precisely the variations in the timing are also key in mmWave communications, as it is in radar. We see that in both systems, the same considerations for the effects of the atmosphere apply, so we will focus on these in this paper.

Many of our simulations involve propagation of signals through a long distance in the atmosphere. Whereas mmWave systems will usually be smaller scale, this is not necessarily the case when a mobile receiver is airborne. When a line of sight exists, the mmWave signals do not fall off much faster than longer wavelengths (scattering is slightly higher). The directionality of the beam helps. The reason that 5G microcells tend to be so small is that shorter wavelengths diffract less than longer wavelengths. This is one of the other active research areas of mmWave [2].

2. THEORETICAL IDEAS: HORIZONTALLY INVARIANT ATMOSPHERE ON A FLAT EARTH

We begin with a simple theoretical model that is based on a flat Earth and an atmosphere with a complex vertical profile of temperature, pressure and water vapor that is independent of location on the Earth. These simplifications will allow us to show that the apparent mobile position will always be at the same horizontal range, i.e., the displacement between the apparent and actual position will be only an altitude difference.

2.1 The classic fisherman's problem

The problem of a fisherman looking into the water at a distance from the bank where he/she stands is inherently a three-dimensional problem. Viewed from the side, Fig. 1, appears to be a standard two-dimensional problem, but the distance of the fish along the refracted ray cannot be determined from this projection. It can be determined from the top view, where the two eyes come into play, and the distance to the fish is determined by that apparent crossing point. The three-dimensional angle is difficult to calculate, but a vector diffraction method makes it simple. The result is that the apparent fish is directly above the real fish. This result can also be determined by the minimum-time principle.

2.2 Generalization

To generalize, we need to consider more than one interface. The simple problem has just one interface at the water surface. When there are multiple interfaces that are all parallel to each other, then the Snell's Law relation $n \sin\theta = n' \sin\theta'$ for index n, n' and angle of incidence to the normal θ, θ' for any two layers. So, consider as many interfaces as is needed to make the vertical profile match the actual profile. The apparent location remains above. This remains true for flat Earth and the vertical profile the same at every point.

The first approximation that we introduce is to perform round Earth ray tracing. This is described in the next section, but it is useful to have the result here. Figure 1b shows a plot of the range error between the mobile location calculated from the standard (dry) atmosphere and the mobile location calculated with the actual profile. We find that the range error is still very small (m at 10's of km). This implies that the result is an extremely good approximation even on a round Earth. In this case, the range is taken as the distance along (parallel to) the surface of the Earth at the given height.

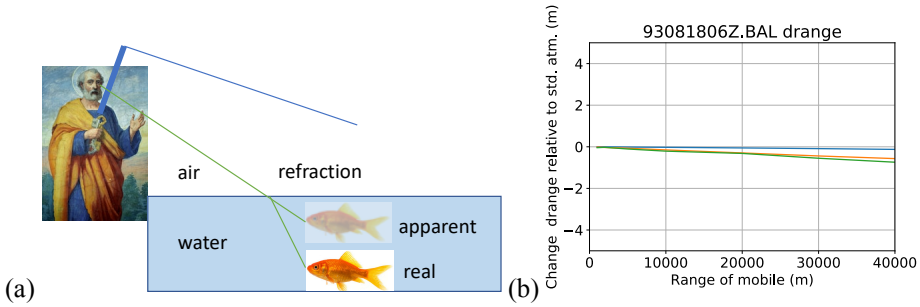

Figure 1. (a) Illustration of 3-dimensional refraction of the fisherman's problem. The side view shows the vertical displacement of the apparent fish. (b) A simulation of a similar problem in a complex vertical, but constant horizontal atmosphere on a round Earth. The small deviations in range (meter in 40 km) relative to the standard atmosphere means that the approximation is good.

3. PHYSICS OF THE EFFECT: REFRACTION

The refractive index can be calculated in terms of the pressure p, water vapor partial pressure e, and temperature T. We begin this section with those relations, then show examples of conversion of vertical profiles of these quantities from rawindsonde measurements to the index of refraction profile. We then show the ray tracing method used to obtain the numerical results.

3.1 Equations for index of refraction

Electromagnetic signals bend towards higher index (n) regions. Thus, gradients of the index of refraction are an important indicator of which way and how strongly the rays will bend. Since gas has a low density of molecules, its index of refraction differs only slightly from $n = 1$. To avoid carrying a large number of decimal places on the index, it is often given in terms of the refractivity N, with index $n = 1 + 10^{-6} N$. The refractivity in terms of our quantities is [3]

$$N = 77.6\frac{p}{T} - 5.6\frac{e}{T} + 3.75 \times 10^5 \frac{e}{T^2} \qquad (1)$$

where the pressures are in [hPa], the temperature in [K] and N is unitless. The e/T term is related to the polarizability of water, while the e/T^2 term is related to the rotation of the permanent dipole moment of water. Thus, N is increased by both pressure and water vapor, while temperature tends to reduce it. The largest effect is usually the pressure dependence with height. This creates enough of a gradient in the refractive index to partially offset the curvature of the Earth, but not completely. Thus, we will still observe an increase of the ray height with distance even when using the US standard atmosphere. Values for p, e and T are obtained from balloon sondes or lidar.

3.2 Index calculation using water vapor and temperature

We now show examples of the results of using these equations. Figure 2(a-b) relates the water vapor altitude profile to the index of refraction profile for a tropical ocean site. There is a strong gradient of the water vapor at ~200-300 meters altitude, which causes a change in the index of refraction. Only the water vapor sonde data are shown, since the pressure follows the adiabatic curve quite closely, and the temperature shows no strong features. The actual values of all three parameters are used to calculate the index. The water vapor is given as a mixing ratio [g/kg], *H2O*, rather than as a water vapor partial pressure e. The conversion to partial pressure is accomplished as $e = \rho * T * H2O/216.7$, where the parameter ρ is the density of the atmosphere.

Another example shown is from the California coast. A layer of dry air from the mountains has inserted itself into the more marine-like air mass, creating a dry layer from ~1500-2600 meters altitude. This causes large gradients in water vapor that influence the index of refraction, Fig 2(c-d). In general, we note that larger gradients occur when dry air blows out over

wet marine airmasses, such as desert air over warm ocean, dry mountain air off CA coast, or similar scenarios at many other worldwide locations.

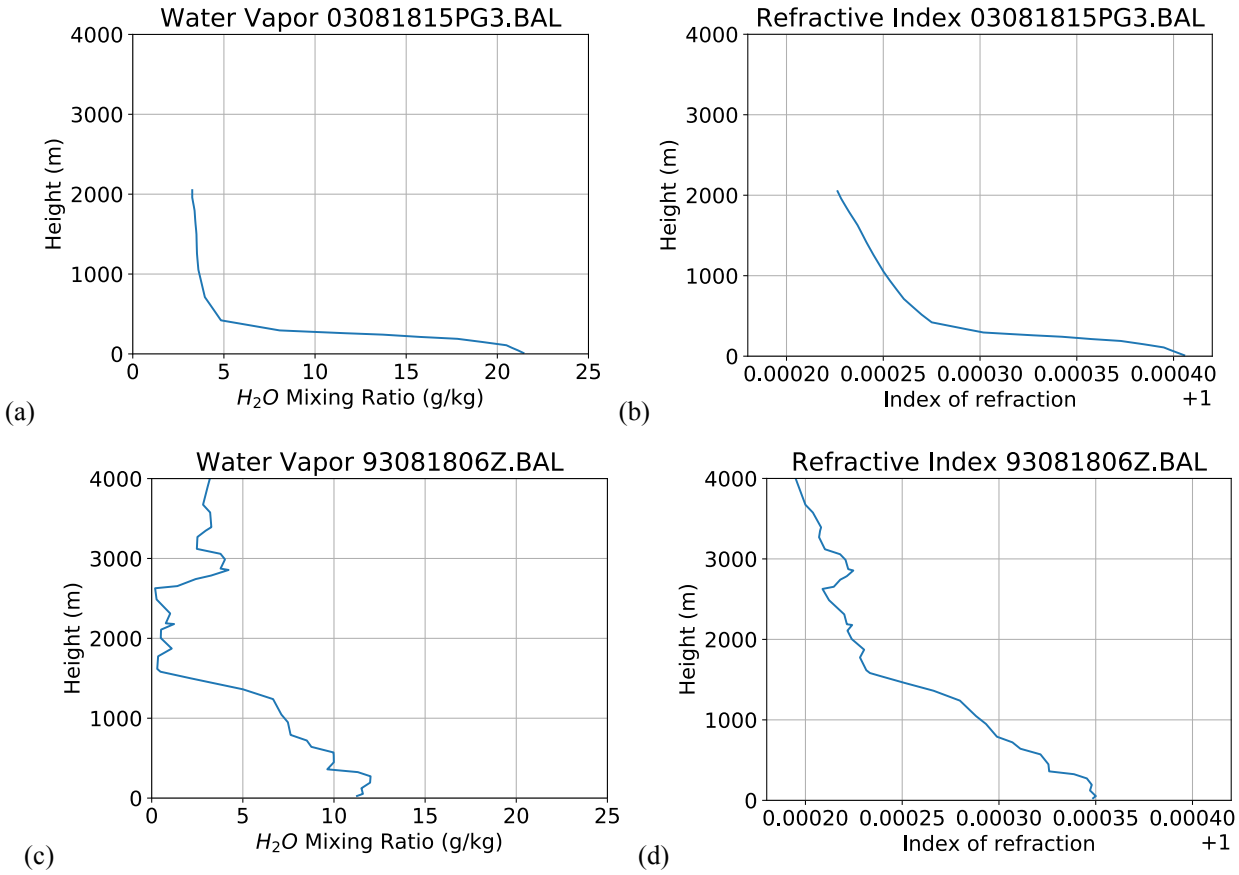

Figure 2. Examples of use of the index calculation formula, Eqn. 1, for measured parameters. The water vapor is shown in parts (a) for a tropical gulf environment, and (c) on the CA coast. The resulting indices of refraction (note the '+1') are given in (b) and (d), respectively.

3.3 Ray tracing equations

Here we calculate the path of a ray given an index of refraction n vs. height, a starting point (ground station/radar) h_0 and ending point (mobile) h_f from Earth's surface, and the range x_f along the Earth's surface of the mobile. To account for the curvature of the Earth, we use polar coordinates, and Snell's Law becomes $n\ r\ \sin(\theta) = n_0\ r_0\ \sin(\theta_0)$ with θ between the radius and the ray being traced. Here, $r_0 = h_0 + R_{Earth}$, and similarly for r. We use R_{Earth} = 6378390 m, g=9.80655 m/s^2, R_{gas} = 287.053 m^{2}s^{-2}C^{-1}. Assuming that the T and the water distribution vs. height is identical at all points along the path, Snell's Law gives us a relation between θ_f and θ_0, but we know neither, so instead we have to vary one until both endpoints are reached with Snell-based ray tracing.

We will ray trace over θ, the angle from the Earth's center, taking $\theta_0 = 0$ and $\theta_f = x/r_0$ [rad]. As we step by $d\theta = dx/r$, the coordinate system rotates so use polar coordinates (r, θ) in the ray tracing formula [4]: $dr/ds = t$; $d(nt)/ds = \text{grad}(n)$ for t tangent to the ray at each point and $ds = dh$ a step along it. In polar coordinates, $dr/ds = \cos(\psi)$; $d(\theta)/ds = \sin(\psi)/r$; $d(\theta+\psi)/ds = -\sin(\psi)/n\ (dn/dr)_{\text{constant }\theta} + \cos(\psi)/(nr)(dn/d\theta)_{\text{const r}}$. The angle ψ is the angle of the ray from vertical at each point. Since we generally only know the values of T and e only at certain x, where they were measured by lidar, for example, we really can't use any a high-powered integration such as Runge-Kutta (our linear interpolation would just undo it); so we go with the simple (not adaptive) step size $ds = dx/\sin(\psi)$ making

$$d(\psi)/ds = -\sin(\psi)/n\ (dn/dr) - d\theta/ds = -dx * (1/r + (dn/dr)/n - 1/(r\tan(\psi))\ (dn/d\theta)/n). \quad (2)$$

The last term is zero for profiles that do not depend upon position. For each step, we update r by $dx/\tan(\psi)$, ψ according to Eqn. 2 (converting ds to dx and multiplying both sides by it), and add $dx\ \mathrm{sqrt}(1+1/\tan^2(\psi))*n/c$ to the propagation delay t for the path, with c the speed of light. In order to take some ideas from Runge-Kutta and improve the accuracy, we actually move through the calculation by taking half the update for r and the delay, t, update ψ, and then do the other half of the r and t update with the new ψ. If we subtract the radius of the Earth from the r's, we have the altitude as a function of position x along the Earth. We will plot these. The delay t is used to determine how far to trace a ray in a standard atmosphere to find the apparent location. The ray tracing, iteration to find the launch angle for the ray to reach the mobile, display and data file input are implemented in Python.

4. SIMULATIONS FOR A LATERALLY CONSTANT ATMOSPHERE

Using the results of the last section, we can take profiles of p, e, and T, along with a radar/base station and mobile position and altitude, and perform simulations.

4.1 Simulation set-up

The first task is to find the actual ray that obeys the ray tracing equations and passes through both the radar and mobile locations. This can only be done by iteration, and that is within our program. The program varies the starting angle until the traced ray intercepts the mobile location. Other rays of interest are: (1) the ray that traverses the Standard Atmosphere and arrives at the mobile target (This ray, compared to the actual, gives the modification of the radar angle compared to what is expected.); (2) the ray that begins with the launch angle of the actual ray, but traverses the Standard Atmosphere for a time equal to the actual ray's total delay time (The endpoint of this ray, the apparent mobile location, compared to the actual mobile position, gives the altitude error and the range error of the apparent vs. actual mobile position.); (3) the tracing of a fan of rays in the actual environment is also useful to gain a qualitative understanding of the ray propagation as a function of range.

Figure 3 shows an example of the calculation of these rays. The presence of a water vapor gradient curves the actual ray further downwards compared to the standard atmosphere. The mobile, at 500 m altitude and 40 km range, is at the intersection of the actual ray and ray (1) above it. As expected from the theoretical result, the apparent mobile is displaced only vertically from the actual mobile position.

We also calculate nearby mobile locations the same way to obtain apparent changes in velocity, vertical size, and signal delay, although we do not show these results in this paper.

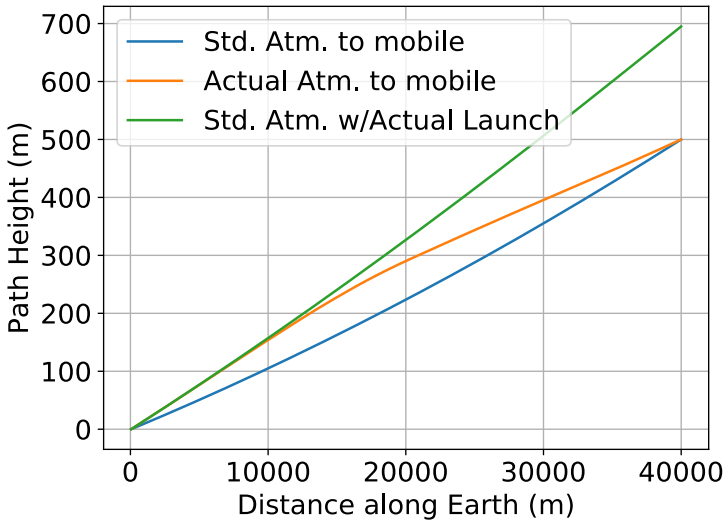

Figure 3. The three rays of interest calculated are shown for a mobile at 500 m altitude and 40 km range.

4.2 Location dependance: four tropical marine sites

For our first example, we want to show that locations not too distant from each other can have strongly different propagation characteristics, Fig. 4. The profiles for p, e, and T were taken at same time and only 1 degree N and W apart.

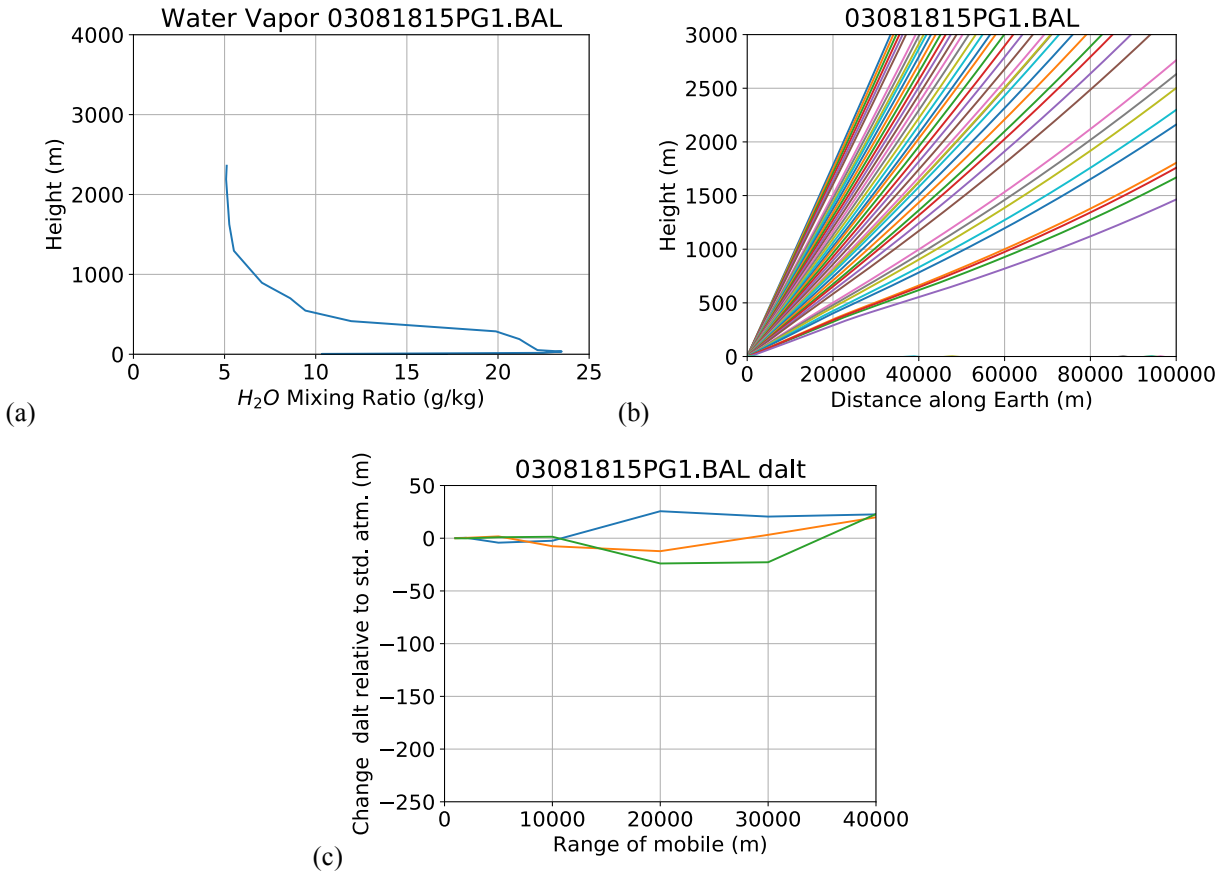

Figure 4. (a) The measured profile of water vapor at the bay entrance. The profiles of pressure and temperature did not differ significantly in altitude from the reference atmosphere, so these are not shown. (b) A fan of rays is traced so that the qualitative effects of the atmosphere can be seen. Note the bending (launch angle dependent) that occurs near the strong gradient in e and n at ~400 m. (c) The altitude errors from a comparison of the apparent and actual mobile location.

We show three plots for each of four locations in Fig. 5. On the left is the water vapor mixing ratio, the center has a traced fan of rays, and the right the apparent altitude error for a mobile at 500 m (blue), 1000 m (orange), 3000 m (green) altitude. The top row is at the bay entrance, and lower rows are further up the bay. There is a weaker gradient at a higher altitude at the bay entrance, and it steepens and appears at a reduced altitude further up the bay. Ducting is apparent in the fan of traced rays and large apparent altitude errors begin with second case. An apparent altitude error of a few hundred meters when the mobile is at 500 m is significant. The smaller altitude errors for larger mobile altitudes is a result of them being further from the height of the strong gradient in the index of refraction.

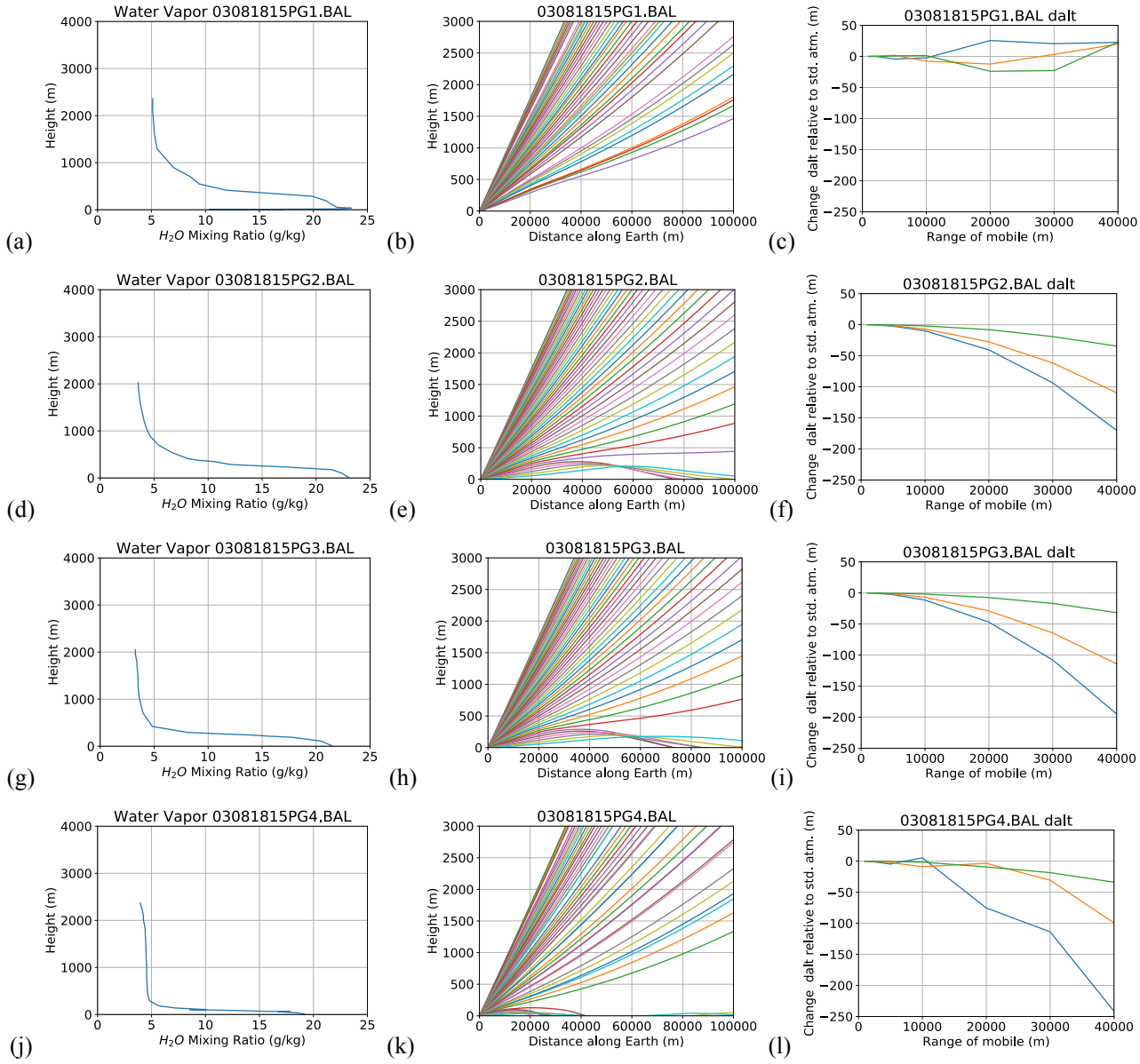

Figure 5. Similar to the last figure, but for several locations. The progression down columns corresponds to positions further up the bay.

4.3 Time dependance: four times in coastal California

For our second example, we want to show that profiles taken at the same location not too long after each other can have strongly different propagation characteristics, Fig. 6. The profiles for p, e, and T were taken at the day/times shown.

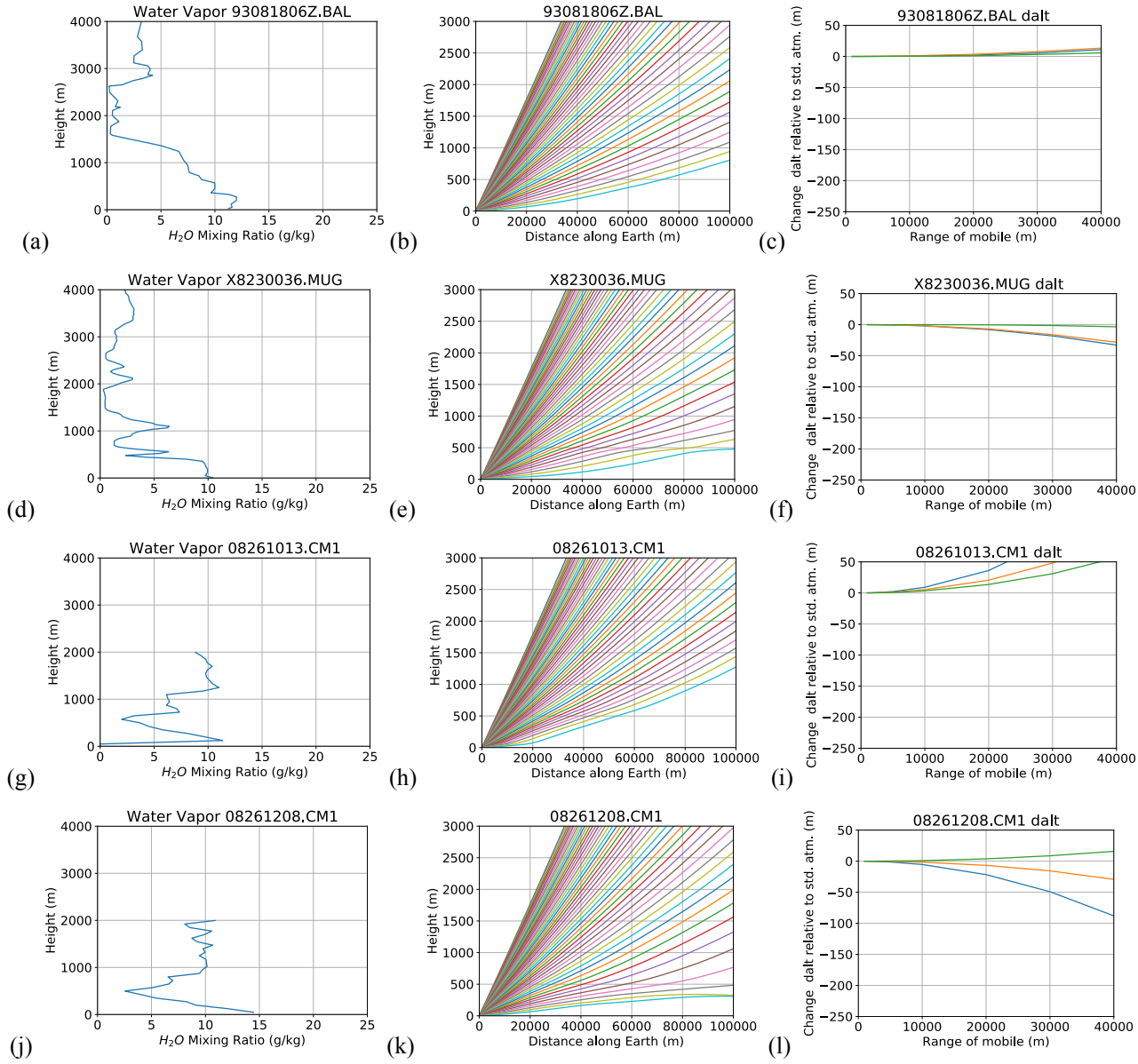

Figure 6. Similar to the last Fig. 4, but for several times at the same location. The progression down columns corresponds to different day/times (GMT). In particular the rows are for 8/18/93 06Z, 8/23/93 00:36Z, 8/26/93 10:13Z, and 8/26/93 12:08Z.

These data were taken at same location over a few days at a location on the California coast. Note the layers of dry air that have blown from the dry mountains to form layers in the otherwise damp marine air, and how they can rapidly change in time. The bottom two are taken only 2 hours apart, yet they have a different sign of altitude error. Further, the bottom one creates different altitude error signs for different altitudes, even on the same profile. The gradients are not quite strong enough to create ducting, which would be visible in the traced fan of rays, but it would not take a much stronger gradient to produce ducting.

5. LIDAR: POSITION DEPENDENT PROFILES

Above, we assumed location-independent profiles of temperature and water vapor. Dry standard atmosphere corrections were done. We still saw interesting effects, the altitude of and angle to the mobile were modified by the atmospheric profile, we observed atmospheric ducting under severe gradients, but as expected, the mobile was only displaced vertically from the apparent location, and the apparent velocity was very close to the actual velocity. Next, we consider the effects of a varying profile with distance. The theoretical idea of only vertical displacement fails. With it fails the inevitability of only vertical displacement and hence an accurate apparent velocity. We show profiles here and comment on how the range errors may accumulate.

Lidar is one of the few tools to provide realistic profiles for testing such possibilities, so we consider these profiles [5].

5.1 Raman lidar profiles, Gulf of Mexico

We begin with an example where the variation of the water vapor has a strong variation in position (time as shown, but as above this can be converted to position with the wind speed). Figure 7 (b) shows a temperature profile that, while not completely constant horizontally, does not contain strong horizontal gradients. We know that the vertical gradients will cause altitude errors only. Figure 7 (a) gives the water vapor profiles. It shows a dry inclusion near 1.5 km altitude, and that the water builds up over the course of the day. The most interesting characteristic, however, is the strong gradient in the horizontal direction for the water vapor at 120 minutes, and several between 200 and 300 minutes. It will result in a horizontal gradient in the index of refraction. This is akin to the fisherman's problem on its side, so will result in range errors.

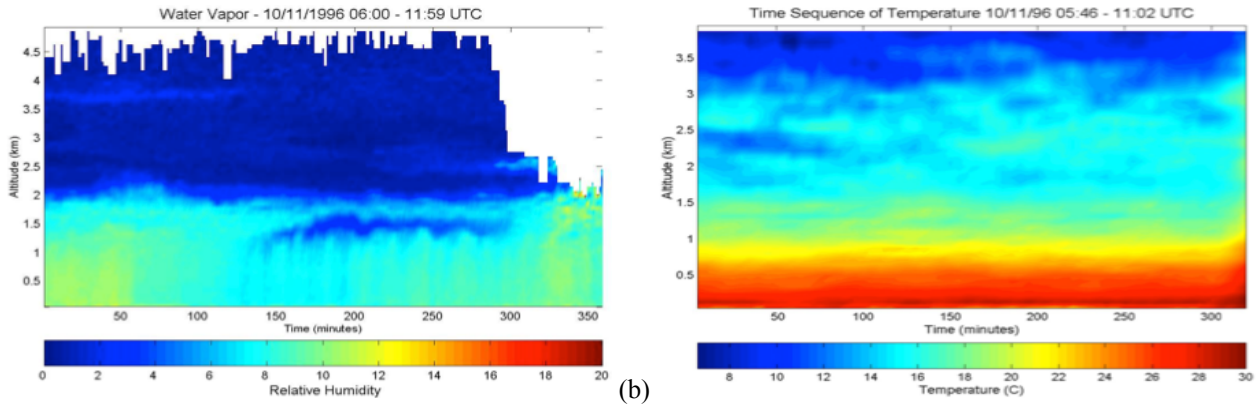

(a) (b)

Figure 7. The (a) water vapor and (b) temperature profiles are shown as a function of time for data taken in the Gulf of Mexico [5-8].

5.2 Raman lidar profiles, Hesparia, CA

Similar observations result from lidar profiles taken in Hesparia, California. Figure 8 shows water vapor as a function of time. The sharp gradient in water vapor is evident in Fig. 8(a), but emphasized in the averaged line-plot Fig. 8(b). The data in part (a) are seen to have variations during the averaging time, so the gradient is even stronger than the line plot suggests. This will give altitude errors primarily, since the dominant variation is in the vertical direction. The altitude of the gradient varies, however, and if one considers a ray that passes through some of the undulations, as it would if it were at a small angle, then large apparent errors in both altitude and range (and other quantities such as apparent mobile speed) would be expected. The data also show that this dry air is a wedge that is being encroached on by damp air from above. Eventually, towards the end of the time period shown, the two set air masses merge. Entrainment of dry air into the upper air mass also created turbulent rolls of dry air within the wet air, visible as yellow dots in the red. These will deflect EM waves. Further, the upper wet air mass has undulations on it, presenting more opportunities for a mobile to move through regions where the path the ground radar or base station passes through strong gradients at man orientations. We would expect strong effects.

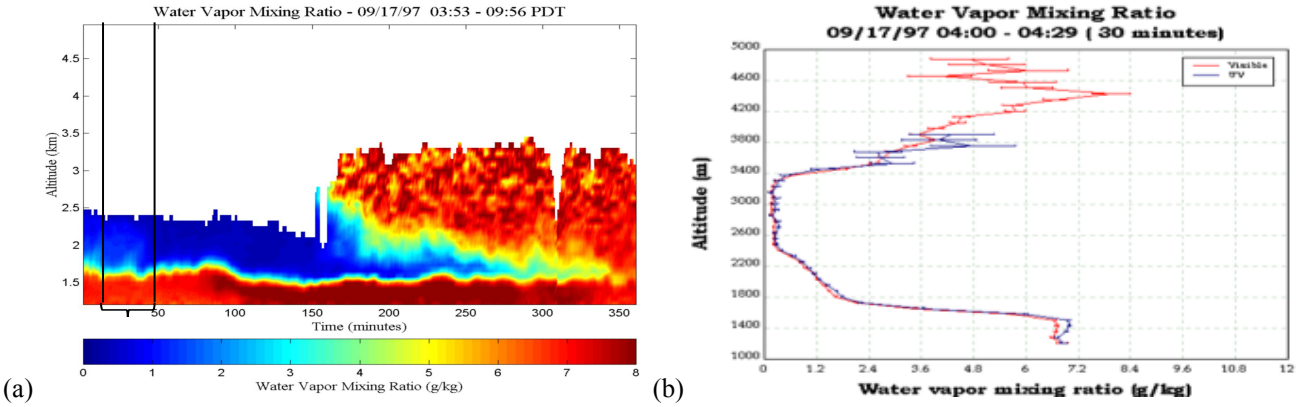

Figure 8. (a) lidar measured water vapor as a function of time in a vertically pointing configuration. (b) Average water vapor mixing ratio from the region in the box in part (a).

5.3 Temperature variation for range errors

Finally, we give an example where the variation of the temperature has a strong variation in position (time as shown, but as above this can be converted to position with the wind speed or sun location). Figure 9(a) shows a water vapor profile that, while not completely constant horizontally, does not contain strong horizontal gradients. We know that the vertical gradients will cause altitude errors only. Figure 9(b) shows a strong gradient in the horizontal direction for the temperature. As for such gradients in water vapor above, it will result in a horizontal gradient in the index of refraction. This is akin to the fisherman's problem on its side, so will result in range errors, showing that both temperature and water vapor can cause such effects.

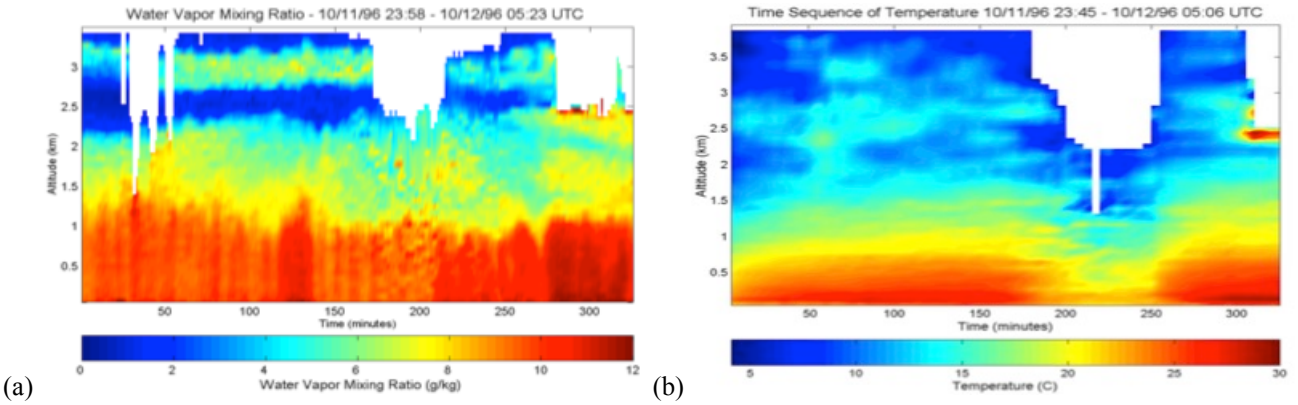

Figure 9. The (a) water vapor and (b) temperature profiles are shown as a function of time for data taken in the Gulf of Mexico.

6. DISCUSSION AND CONCLUSIONS

The electromagnetic signal beam path in horizontally invariant atmospheres shows ducting and strong refractive effects that can vary in position and in time, but the apparent position remains close to the same range, with altitude variation. The models assume that a correction will be made for a standard dry atmosphere, which accounts for a large refraction on its own. These cases are shown in round-Earth ray tracing with real atmospheric profiles. The next step is to take Raman

lidar data profile series for refraction to understand the impacts of realistic variations of the water vapor and temperature, hence index of refraction, on position, using the same ray tracing engine. We expect the large variations shown in our prior lidar data will result in refraction that introduces variable range errors, hence apparent speed errors, from the perspective of the ground unit. These conclusions apply to radars used for detection of direction and range, and communications systems to airborne mobile units requiring low pointing error and phase tracking.

These studies aim to answer the question of what it means when you get a signal from a particular direction with a measured delay time.

REFERENCES

[1] U.S. Standard Atmosphere, 1976, Superintendent of Government Documents, US Government Printing Office, Washington DC 20402

[2] Ali, Z., Duel-Hallen, A. and Hallen, H., "Early Warning of mmWave Signal Blockage and AoA Transition Using sub-6 GHz Observations," IEEE Commun. Lett. 24(1), 207–211 (2020).

[3] Smith, E. K. and Weintraub, S., "The Constants in the Equation for Atmospheric Refractive Index at Radio Frequencies," Proceedings of the IRE 41(8), 1035–1037 (1953).

[4] Auer, L. H. and Standish, E. M., "Astronomical Refraction: Computational Method for All Zenith Angles," AJ 119(5), 2472–2474 (2000).

[5] Philbrick, C. R. and Hallen, H. D., "Lidar investigations of atmospheric dynamics," Proc. SPIE 9612, Lidar Remote Sensing for Environmental Monitoring XV, 96120C (1 September 2015).

[6] Philbrick, C. R. and Hallen, H. D., "Laser remote sensing of species concentrations and dynamical processes," Laser Radar Technology and Applications XIX; and Atmospheric Propagation XI, Vol. 9080, SPIE Proceedings, 2014

[7] Philbrick, C. R., Hallen, H. D., Snyder, M. G., and Brown, A. M., "Remote sensing of atmospheric aerosol properties," Proceedings of 13th Conference on Atmospheric Chemistry, Vol. J11.3, American Meteorological Society, 2011, pp. 1-13.

[8] Philbrick, C. R., Hallen, H. D., Wyant, A. M., Wright, T., and Snyder, M. G., "Optical remote sensing techniques characterize the properties of atmospheric aerosols," Laser Radar Technology and Applications XV, Vol. 7684, SPIE, 2010.